

Laminar and Turbulent Shear-Induced Flocculation of Fractal Aggregates

Jürgen C. Flesch, Patrick T. Spicer, and Sotiris E. Pratsinis

Dept. of Chemical Engineering, University of Cincinnati, Cincinnati, OH 45221

A population balance model is used to model simultaneous coagulation and fragmentation in turbulent shear. The fractal-like aggregate structure is quantified using a mass fractal dimension, $D_f = 2.05$, derived from light-scattering measurements and is incorporated into the model using appropriate kinetic expressions. In addition, fluid viscous effects on aggregate collisions are taken into account using existing theories on viscous retardation. Flocculation experiments of a polystyrene particle/ $\text{Al}(\text{OH})_3$ /water system in a stirred tank are compared to the model results. Good agreement is found for both average-size evolution and steady-state size distribution using only one fitting parameter and assuming binary breakage. The average polystyrene- $\text{Al}(\text{OH})_3$ aggregate size initially increases before reaching a constant steady-state value during coagulation-fragmentation in a stirred tank. Increasing the applied shear rate increases the coagulation and fragmentation rates, decreasing the steady-state average aggregate size, and the time lag before steady state. The model developed in this work is applied to laminar shear data from the literature, showing excellent agreement.

Introduction

Particle removal from suspension in a liquid is relevant to numerous areas of research and industry. The efficient recovery of commodity particulate products requires the efficient sedimentation and/or filtration of particles from a suspending liquid. Flocculation is often facilitated in a stirred tank where the distribution of velocity gradients brings the particles close enough to collide. If added flocculants suppress repulsive interactions between particles and the inertia of approaching particles overcomes fluid viscous resistance, a collision results in the formation of an aggregate.

Irregular, fractal aggregates form during shear-induced collisions when particles adhere to one another in their instantaneous random orientations, increasing the average particle size (Mandelbrot, 1983; Klimpel and Hogg, 1986; Meakin, 1988). These aggregates have a much larger collision profile than their volume equivalent spherical counterparts, which enhances collision rates (Tambo and Watanabe, 1979a; Jiang and Logan, 1991; Wiesner, 1992) and reduces the fluid

viscous resistance to collisions (Kusters et al., 1997). Hierarchical simulations of aggregate-aggregate collisions predict a fractal dimension, $D_f = 1.8$, while particle-cluster collisions produce a more compact $D_f \sim 3$ (Torres et al., 1991), although particle-cluster collisions will only alter realistic aggregate structures to a small extent ($D_f = 2$) (Kusters et al., 1997). Porous aggregates are fragmented by fluid shear stresses more rapidly than compact mass equivalent particles (Adler and Mills, 1979) at a rate dependent on the applied shear rate, the aggregate structure, and the bonds between primary particles (Sonntag and Russel, 1986, 1987; Potanin, 1991; Horwatt et al., 1992). Aggregate restructuring to a more compact form may also occur by reaggregation of fragments (Clark and Flora, 1991; Spicer et al., 1998), or by shear interactions that rearrange the structure (Oles, 1992).

After a characteristic time, a steady state is reached between coagulation and fragmentation, characterized by an aggregate size distribution that does not change with time and is unique for a given system (Spicer and Pratsinis, 1996a). Accurate particle flocculation models must incorporate the dependency of flocculation kinetics on aggregate structure, the fluid shear field, and their mutual interactions. Previous

Correspondence concerning this article should be addressed to P. T. Spicer.
Present address of P. T. Spicer: The Procter and Gamble Company, Este Process Technology Center, 4530 Este Avenue, Cincinnati, OH 45232.

studies of fractal aggregate dynamics in stirred tanks modeled only short residence times and ignored fragmentation and viscous effects.

The objective of this work is to study the effect of aggregate structure on simultaneous shear-induced coagulation and fragmentation using appropriate kinetic expressions. Existing work on aggregate collision and fragmentation rates is used to accurately model flocculation behavior. Comparisons are made with experimental data for the evolution of aggregate size and structure in a stirred tank, and conclusions are drawn as to the accuracy of assuming a constant fractal dimension for a flocculating particle suspension.

Theory

Population balance model

Simultaneous coagulation and fragmentation can be modeled by population balance techniques. The rate of change of the particle number concentration by coagulation and fragmentation is given by (Hounslow et al., 1988; Spicer and Pratsinis, 1996a):

$$\begin{aligned} \frac{dN_i}{dt} = & N_{i-1} \sum_{j=1}^{i-2} 2^{j-i+1} \alpha_{i-1,j} \beta_{i-1,j} N_j \\ & + \frac{1}{2} \alpha_{i-1,i-1} \beta_{i-1,i-1} N_{i-1}^2 - N_i \sum_{j=1}^{i-1} 2^{j-i} \alpha_{i,j} \beta_{i,j} N_j \\ & - N_i \sum_{j=i}^{\max_1} \alpha_{i,j} \beta_{i,j} N_j - S_i N_i + \sum_{j=i}^{\max_2} \Gamma_{i,j} S_j N_j, \quad (1) \end{aligned}$$

where N_i represents the number concentration of aggregates containing 2^{i-1} primary particles; the factor α represents the collision efficiency accounting for hydrodynamic interactions between colliding particles; $\beta_{i,j}$ denotes the collision frequency for particles of volume i and j ; S_i is the fragmentation rate of aggregates of size i ; and $\Gamma_{i,j}$ represents the breakage distribution function defining the volume fraction of the fragments of size i coming from j -sized particles.

In Eq. 1, the first two terms on the righthand side (RHS) represent the formation of particles by size i by the collision of particles from sections smaller than section i . The third and fourth RHS term denote the loss of particles of size i by coagulation with those of another size. The fifth term describes the loss of particles of size i by fragmentation, and the sixth RHS term describes the formation of particles of size i by fragmentation of larger particles. For each section, one equation has to be solved. The use of $\max_1 = 30$ sections was sufficient to cover the size range used in this research (Spicer and Pratsinis, 1996a).

Aggregate structure

Aggregates formed by flocculation usually do not have a spherical shape, but rather a more irregular structure. The expression of fractal dimension was proposed by Mandelbrot (1987) and is useful to describe the irregularity of self-similar aggregates, even though in reality aggregates lack an *exact* fractal structure. Experiments have shown that the aggregates

formed by shear coagulation are usually fractal-like (Schmidt-Ott et al., 1990; Oles, 1992). In order to quantify this structure, the fractal dimension of an aggregate is used here.

The mass fractal dimension, D_f , describes the relationship between the characteristic length, l , of an aggregate and its mass, M :

$$M \propto l^{D_f}. \quad (2)$$

The value of D_f varies from 1 (an aggregate made from a line of particles) to 3 (for compact spherical-shaped aggregates). The collision or maximum radius, R_c , of an aggregate will determine aggregation kinetics and is a function of its fractal dimension:

$$R_{c,i} = R_0 \left(\frac{i}{k} \right)^{1/D_f}, \quad (3)$$

where k is the lacunarity, a form of packing density, and here $k = 1$ is used (Wiesner, 1992; Kusters et al., 1997). From Eq. 3 it is clear that the smaller the D_f , the more openly structured the aggregate is and the larger its collision profile. This larger collision profile impacts the kinetics of the flocculation process.

Coagulation

The orthokinetic coagulation collision frequency, β , was derived by Saffman and Turner (1956) for the binary collision of spherical particles smaller than the Kolmogorov microscale, η , in homogeneous, isotropic turbulence:

$$\beta_{i,j} = 1.294 \left(\frac{\epsilon}{\nu} \right)^{1/2} (R_{c,i} + R_{c,j})^3, \quad (4)$$

where ϵ represents the homogeneous turbulent energy dissipation rate of the stirred tank; ν is the kinematic viscosity of the suspending fluid; and the square root of their ratio is often referred to as a "volume averaged shear rate," G . Equation 4 is easily modified to account for the effect of aggregate structure on collision frequency (Jiang and Logan, 1991):

$$\beta_{i,j} = 1.294 R_0^3 k^{-3/D_f} G (i^{1/D_f} + j^{1/D_f})^3. \quad (5)$$

As shown in the preceding equation, R_0 represents the primary particle radius. A similar form of the collision frequency is known for laminar shear flow due to Smoluchowski (1917); this form is obtained by replacing the numerical constant (1.294) in Eq. 5 with $4/3$ and G with $\dot{\gamma}$, the linear shear rate.

Viscous retardation

As two spherical particles approach one another in fluid shear, the viscous fluid layer between them resists collision, in some cases completely (Adler, 1981b). Porous aggregate structures restrict fluid flow less than spheres (Adler, 1981a),

decreasing the viscous resistance (Kusters et al., 1997). In the population balance equation, viscous resistance is reflected in the collision efficiency, α , the ratio of the actual collision frequency, and the collision frequency in the case that every collision is assumed to be successful. Therefore, depending on the strength of the viscous retardation, α will have values between 0 and 1. Kusters et al. (1997) developed a model to calculate the aggregate collision efficiency by representing aggregates as dense cores surrounded by porous shells, calculating the permeability based on a fractal model of aggregate structure, and using the trajectory calculations of Adler (1981a,b). The detailed model of Kusters et al. (1997) has been implemented here to account for the reduction in collision frequency by viscous effects.

Fragmentation

The disruption of aggregates is caused by hydrodynamic stresses. The larger an aggregate becomes, the more susceptible it is to breakage. The fragmentation rate given by Kusters (1991) has its origin in the work of Delichatsios and Probst (1976):

$$S_i = \left(\frac{2}{\pi}\right)^{1/2} \frac{\Delta u}{a_i} \exp\left(\frac{-\Delta u_b^2}{\Delta u^2}\right), \quad (6)$$

where Δu is the rms velocity difference across the distance a_i , and Δu_b is the critical velocity difference at which breakage occurs. Substituting for Δu and Δu_b in Eq. 6 gives the simplified form of the fragmentation rate (Kusters, 1991):

$$S_i = \left(\frac{4}{15\pi}\right)^{1/2} \left(\frac{\epsilon}{\nu}\right)^{1/2} \exp\left(\frac{-\epsilon_{b,i}}{\epsilon}\right), \quad (7)$$

where $\epsilon_{b,i}$ is the critical turbulent energy dissipation rate at which the aggregates fragment.

Since larger particles are more susceptible to turbulent shear stresses, the value of $\epsilon_{b,i}$ must be related to the aggregate size in a way consistent with the findings that $\epsilon_{b,i}$ decreases with increasing aggregate size. A power-law relationship between aggregate size and shear rate is commonly used to correlate experimental (Tambo and Watanabe, 1997b) and simulation results (Potanin, 1991):

$$R_{c,i} \propto G^{-m}, \quad (8)$$

where m varies between 0.4 and 4 for turbulent flow and various aggregate types (Thomas, 1964; Tomi and Bagster, 1978; Tambo and Watanabe, 1979b; Francois, 1987). The theory of irregular aggregate fragmentation is not as definite as that for shear-induced coagulation. As a result, it is sufficiently accurate to choose an expression that is physically significant and that describes experimental data based on Eq. 8:

$$\epsilon_{b,i} = BR_{c,i}^{-2/m}, \quad (9)$$

where B is a fitting parameter and $m=2$, consistent with the average result found experimentally and the expectation that breakage will depend on the linear aggregate dimension.

Equation 9 predicts an inverse relationship between energy dissipation rate and aggregate size: as aggregates grow larger they are more susceptible to fragmentation by fluid shear. The effect of aggregate structure is also included by the use of the collision radius, $R_{c,i}$, as a measure of aggregate size that increases with decreasing D_f . The use of the collision radius in the preceding equation thus accounts for the larger profile of fractal aggregates vs. spherical equivalent particles. Two fragment size distribution functions are examined. Binary fragmentation describes the breakage of an aggregate into two equal fragments:

$$\Gamma_{i,j} = \frac{v_j}{v_i}, \quad \max_2 = i+1, \quad (10)$$

while a second case produces a normal distribution of fragments (Spicer and Pratsinis, 1996a):

$$\Gamma_{i,j} = \frac{v_j}{v_i} \int_{b_{i-1}}^{b_i} \frac{1}{\sqrt{2\pi}\sigma_f} \exp\left(-\frac{(v-v_{fa})^2}{2\sigma_f^2}\right) dv, \quad \max_2 = \max_1, \quad (11)$$

where v_{fa} is the mean volume of the fragment size distribution (half the volume of the fragmenting aggregate), σ_f is the standard deviation of the fragment size distribution:

$$\sigma_f = \frac{v_f}{\lambda}, \quad (12)$$

where v_i is the aggregate undergoing fragmentation and λ is a variable that, when decreased, broadens the fragment size distribution (Spicer and Pratsinis, 1996a).

Experimental Study

Flocculation of an aqueous suspension of monodisperse, spherical, polystyrene particles ($d_0 = 0.87 \mu\text{m}$) was studied in a 2.8 liter, baffled, stirred tank of standard configuration (Spicer and Pratsinis, 1996b). The suspension was mixed using a radial flow (Rushton) Lightnin R100 impeller. The center of the impeller was positioned at one-third the height of the tank. The solids volume fraction, ϕ_p , was set equal to 1.4×10^{-5} , corresponding to an initial number concentration of $4 \times 10^7 \text{ cm}^{-3}$. The flocculant was aluminum sulfate hydrate ($\text{Al}_2(\text{SO}_4)_3 \cdot 16\text{H}_2\text{O}$; Aldrich 98%) (Clark and Flora, 1991). All experiments were conducted using a constant $\text{Al}_2(\text{SO}_4)_3 \cdot 16\text{H}_2\text{O}$ concentration of 10 mg/L. Sodium hydrogen carbonate (NaHCO_3 ; Aldrich, 99%), at a concentration of 1 mM, was used to buffer the suspension, and the pH was kept at 7.2 ± 0.05 during all experiments. The buffered polystyrene suspension was first mixed at $G = 300 \text{ s}^{-1}$ for 5 min to break up any agglomerates. The flocculant was then added and mixed with the suspension for one minute and the impeller was set to the desired speed. The impeller rotational velocity was measured using an optical tachometer (Onno Sokki MT-4100) and varied by less than 1 rpm. All experiments were carried out 2 to 3 times; very little variation was observed between runs. The turbulent shear rate within the

stirred tank was characterized using the volume-averaged gradient, G , following the procedures of Spicer and Pratsinis (1996b).

The samples taken during flocculation were gently withdrawn from the tank into the Malvern flowthrough sample cell using a syringe (Ng et al., 1993). In all cases, samples were withdrawn from the same location in the tank, midway between the impeller and the top of the suspension. Although a large number of particles (> 500) had to be withdrawn to accurately determine an aggregate size distribution, care was taken not to alter fragile aggregate structures by sampling procedures (Spicer et al., 1998).

Small-angle light-scattering measurements by a Malvern Mastersizer E (Malvern Instruments) were used to evaluate the aggregate-size distribution and the average aggregate structure and density as a function of time. The structure of the aggregates was determined quantitatively by their mass fractal dimension, D_f . The scattering behavior of suspended particles is dependent on the ratio of primary particle size, d_0 , to the wavelength of light scattered, λ_{Laser} , so that if

$$d_0 \gg \lambda_{\text{Laser}}, \quad (13)$$

(as is the case here) the fractal dimension, D_f , is determined from the slope (slope = $D_f - 3$) of a log-log plot of the ratio of the initial suspended particle volume fraction, ϕ_p , to that of the flocculated suspension, ϕ_f , vs. the mass mean collision diameter, $d_{c,mm}$, of the floc size distribution based on rearrangement of Eqs. 2 and 3 (Oles, 1992; Kusters et al., 1997):

$$\frac{\phi_p}{\phi_f} \propto d_{c,mm}^{D_f-3}. \quad (14)$$

The apparent volume fraction of the suspended aggregates is a function of the obscuration (OB) of the laser beam, a parameter reported by the Mastersizer (Kusters, 1991; Kusters et al., 1997):

$$\phi_f = \frac{d_{sm} \ln(1 - OB)}{3L}, \quad (15)$$

where d_{sm} is the Sauter mean diameter of the size distribution (Kusters et al., 1997), and L is the laser path length (2.1 mm). This structural characterization technique allows measurement of the average aggregate fractal dimension over the experiment duration. Characterization of aggregate restructuring is also possible when multiple slopes are present (Oles, 1992).

Results and Discussion

In order to model the experimental light-scattering size distribution data, the population balance model (Eq. 1) was solved using the collision frequency function of Eq. 5, the fragmentation rate of Eq. 7, and the collision efficiency calculated using the shell-core model of Kusters et al. (1997). It was assumed that the aggregates split into two equal-sized fragments (binary breakage) (Spicer and Pratsinis, 1996a) unless otherwise specified.

The initial particle-size distribution of the suspension at the defined beginning of the flocculation simulation ($t=0$) was not monodisperse, although monodisperse polystyrene particles were added to the tank. For homogeneous distribution in the tank, the alum flocculant was mixed with the suspension for one minute at high shear rate. Inevitably, some flocculation will occur during this time. Thus, since not all the initial conditions can be known with certainty, the aggregate-size distribution measured following the rapid mixing period was used as the initial condition in all simulations of stirred-tank data. Since the model particle-size range discretization is different from that by the Malvern instrument, an initial size distribution was evaluated for agreement with the measured one and implemented into the model. Both measured and evaluated theoretical initial size distributions are shown to agree nicely in Figure 1 using the normalized volume fraction (Hinds, 1982):

$$q_{3,i} = \frac{N_i V_i}{\Delta d_{c,i} \sum_i N_i V_i}, \quad (16)$$

where $\Delta d_{c,i}$ is the width of section i .

The objective of this work is to model aggregate flocculation dynamics using a quantitative description of aggregate structure. Structural characterization of the aggregates is also possible using light-scattering techniques. Figure 2 shows a log-log plot of the evolution of the average aggregate density

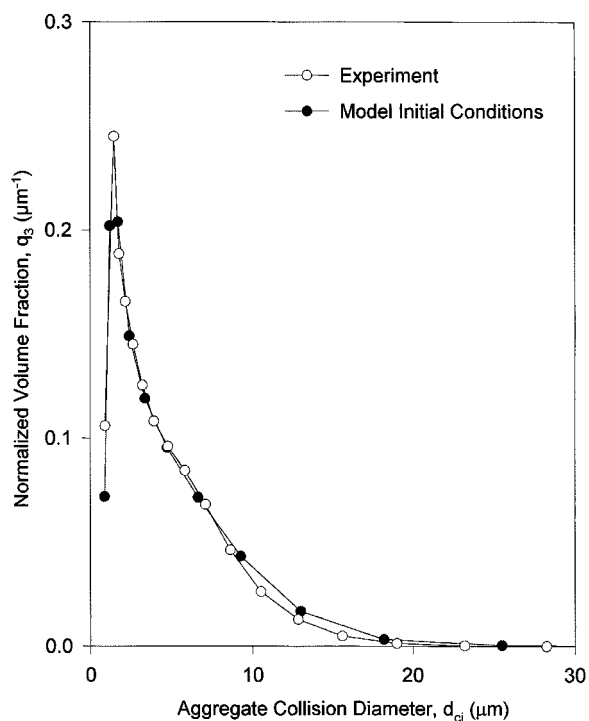


Figure 1. Initial aggregate size distribution measured after 1 min of rapid mix at $G = 300 \text{ s}^{-1}$ (open circles).

Also shown is the distribution used as the model's initial conditions (filled circles).

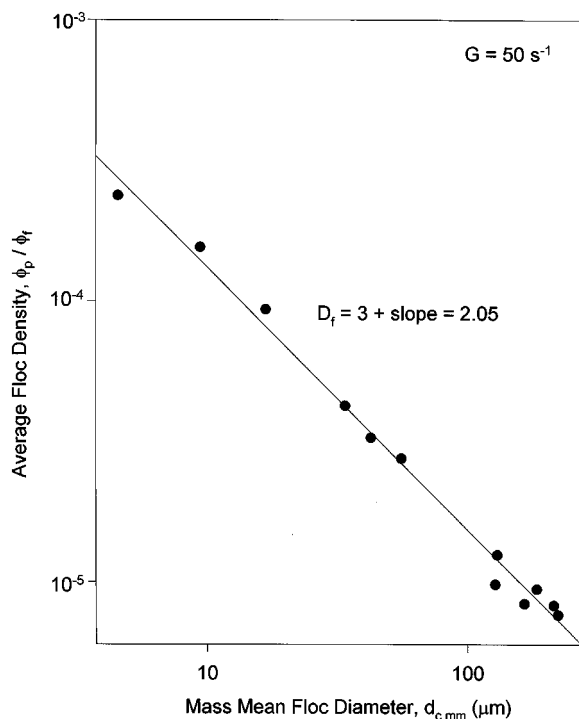


Figure 2. Determination of the average aggregate mass fractal dimension via Eq. 14 and the change in average aggregate density.

The slope of a regression line through the data provides the value of D_f (Kusters et al., 1997).

ratio, ϕ_p/ϕ_f , and the mass mean diameter. Equation 14 can be used to determine the time-averaged fractal dimension from the slope of a regression line through the data points in Figure 2. Analysis of all three shear rates resulted in a fractal dimension of $D_f = 2.05 \pm 0.05$. This value is in excellent agreement with the early stages of laminar (Oles, 1992) and turbulent (Spicer et al., 1998) shear-induced aggregation.

Effect of aggregate structure on flocculation kinetics

The larger collision profile of aggregates relative to spheres enhances their collision frequency (Eq. 5). As a result, decreasing the aggregate fractal dimension, D_f , will have a significant effect on flocculation kinetics. Figure 3 shows the calculated evolution of the mass mean aggregate collision diameter with time as a function of D_f . The results represented by the lines in Figure 3 were calculated assuming coagulation only was operative, that is, Eq. 7 (the fragmentation rate) was set to zero. This serves to highlight the behavior of the model at short times before fragmentation becomes significant, while at long times (i.e., $t > 10$ min) the need for a description of fragmentation in the model becomes evident. In Figure 3, at all values of D_f , the aggregate size increases exponentially with time, consistent with previous experimental (Oles, 1992; Spicer et al., 1998) and theoretical work on this collision mechanism (Vigil and Ziff, 1989). A dramatic enhancement in the calculated aggregate growth rate is seen in Figure 3 as D_f as decreased from 2.15 to 2.05 to 1.95, increasing the mass mean aggregate size by as much as a fac-

tor of 3 at a given time. From Figure 3 it is also clear that these values of D_f will substantially increase aggregation rates vs. a spherical model of aggregation ($D_f = 3$), indicating the necessity of accounting for aggregate structural enhancement when modeling aggregation data. Finally, in Figure 3 the measured $D_f = 2.05$ results in excellent agreement between model and experiment for pure coagulation (short times) at $G = 50 \text{ s}^{-1}$. It is worth noting here that no fitting has been used to obtain the result in Figure 3, the fractal dimension was measured experimentally and incorporated into the model via Eqs. 1 and 5 and the viscous interaction model of Kusters et al. (1997).

Aggregate fragmentation

In order to break up an aggregate, there is a certain minimum energy dissipation rate that must be present in the heterogeneous turbulent shear field. As shown in Eq. 9, the critical energy dissipation rate is inversely proportional to the aggregate collision radius. The fitting parameter, B , is used to adjust the absolute strength of fragmentation based on the steady-state value of the mass mean diameter. An example of such adjustment is shown in Figure 4 for $G = 150 \text{ s}^{-1}$. In Figure 4, coagulation dominates the beginning of the experi-

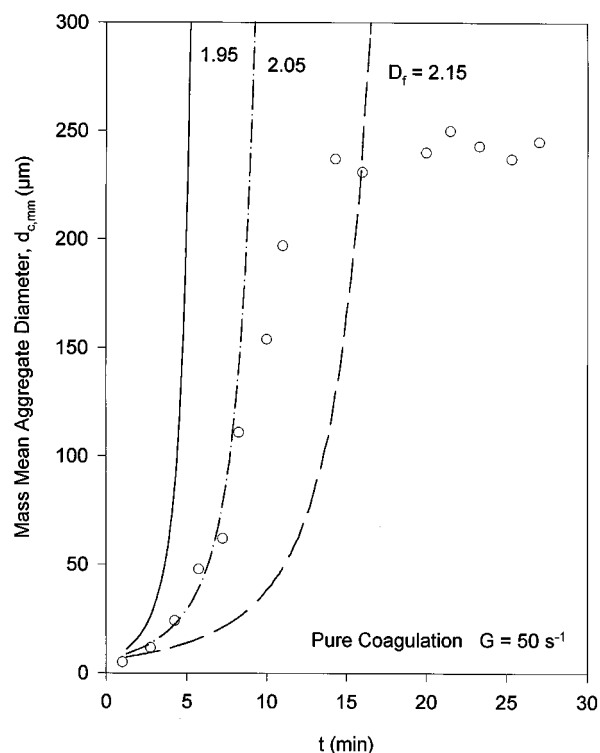


Figure 3. Calculated effect of the average mass fractal dimension, D_f , on the mass mean aggregate size (three lines) during the aggregation-dominated regime (solution of Eq. 1 with Eq. 7 set to zero).

Open circles indicate experimental data for $G = 50 \text{ s}^{-1}$. A decreased fractal dimension reflects an increased aggregate linear dimension (Eq. 3), producing a greater relative rate of shear-induced collisions for the same aggregate mass.

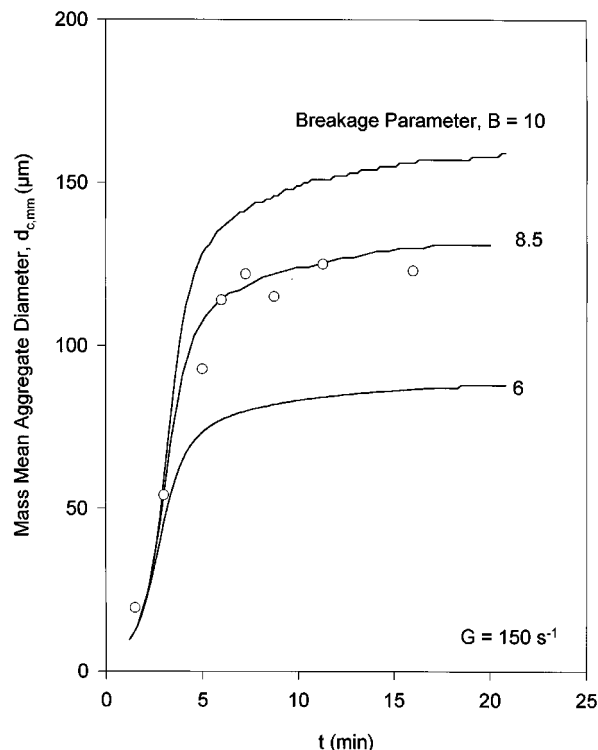


Figure 4. Determination of the breakage parameter, B , in Eq. 9 by comparison of calculated size evolution (solid lines) with experimental data (open circles).

Increasing values of B decrease the fragmentation rate (relative to the aggregation rate) for a given shear rate, increasing the steady-state mass mean aggregate size.

ment and fragmentation is nearly negligible (i.e., the curves are the same independent of the value of B). With time, however, aggregates become larger and more susceptible to fluid shear stresses, and fragmentation increases in significance. The larger the fragmentation rate or the lower the necessary energy dissipation rate (low B), the earlier fragmentation begins. For this case, $B=10$ overpredicts the steady-state results (breakage is too weak), while $B=6$ underpredicts them (breakage too strong). When $B=8.5$ is used, the predicted and measured steady-state data agree well.

Comparison of model and experiment

Figure 5 shows the predicted (lines) and experimental (markers) time evolution of the mass mean aggregate collision diameter, $d_{c,mm}$ for the three shear rates $G=50, 100,$ and 150 s^{-1} . For all three shear rates, an initial increase of particle size is observed as a result of the coagulation process. After a certain time, fragmentation becomes more significant as the aggregates become larger. Fragmentation slows down the aggregate growth and a steady state is eventually reached between coagulation and fragmentation, allowing no further growth. This is consistent with experimental observations of turbulent (Spicer and Pratsinis, 1996b) and laminar (Oles, 1992) shear-induced flocculation. From Figure 5 it can be seen that higher shear rates lower the steady-state mean

aggregate size. Although a shift to higher shear rates increases the coagulation rate, fragmentation is also more significant with increasing shear rate, opposing coagulation more rapidly and decreasing the time lag before attainment of steady state (Spicer, 1998). The model describes experimental data very well for all three shear rates at all stages of the flocculation process, from the very early coagulation to the achievement of steady state. The value of B was fitted for each shear rate ($B=1.7$ for $G=50$; $B=4.8$ for $G=100$; and $B=8.5$ for $G=150 \text{ s}^{-1}$).

Steady-state size distribution

It can be seen from Figure 5 that the model is in good agreement with the experimental data regarding mass mean diameter evolution. Since this is only an averaged value, it is of interest to compare the model predictions with the full experimental steady-state size distributions. Figure 6 compares theoretical (lines) and experimental (symbols) steady-state size distributions at the three different shear rates studied here [$G=50$ (part a), 100 (part b), and 150 (part c) s^{-1}]. Observation of the experimental data indicates that the higher the shear rate, the narrower the distributions and the more they are shifted to smaller aggregate sizes as a result of higher

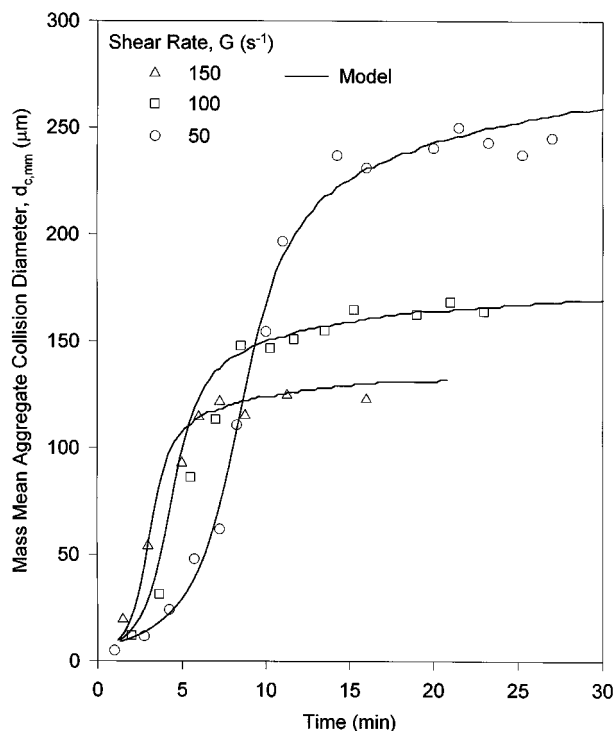


Figure 5. Calculated (solid lines) vs. experimental (symbols) time evolution of the mass mean aggregate size in turbulent shear as a function of the average shear rate, G .

For model (solution of Eq. 1) and experiment, aggregate size initially increases rapidly while aggregation dominates, then slows and reaches a constant steady-state value, as fragmentation becomes significant. Increasing shear brings about increased fragmentation, decreasing the steady-state aggregate size. The model is in excellent agreement with the experimental results.

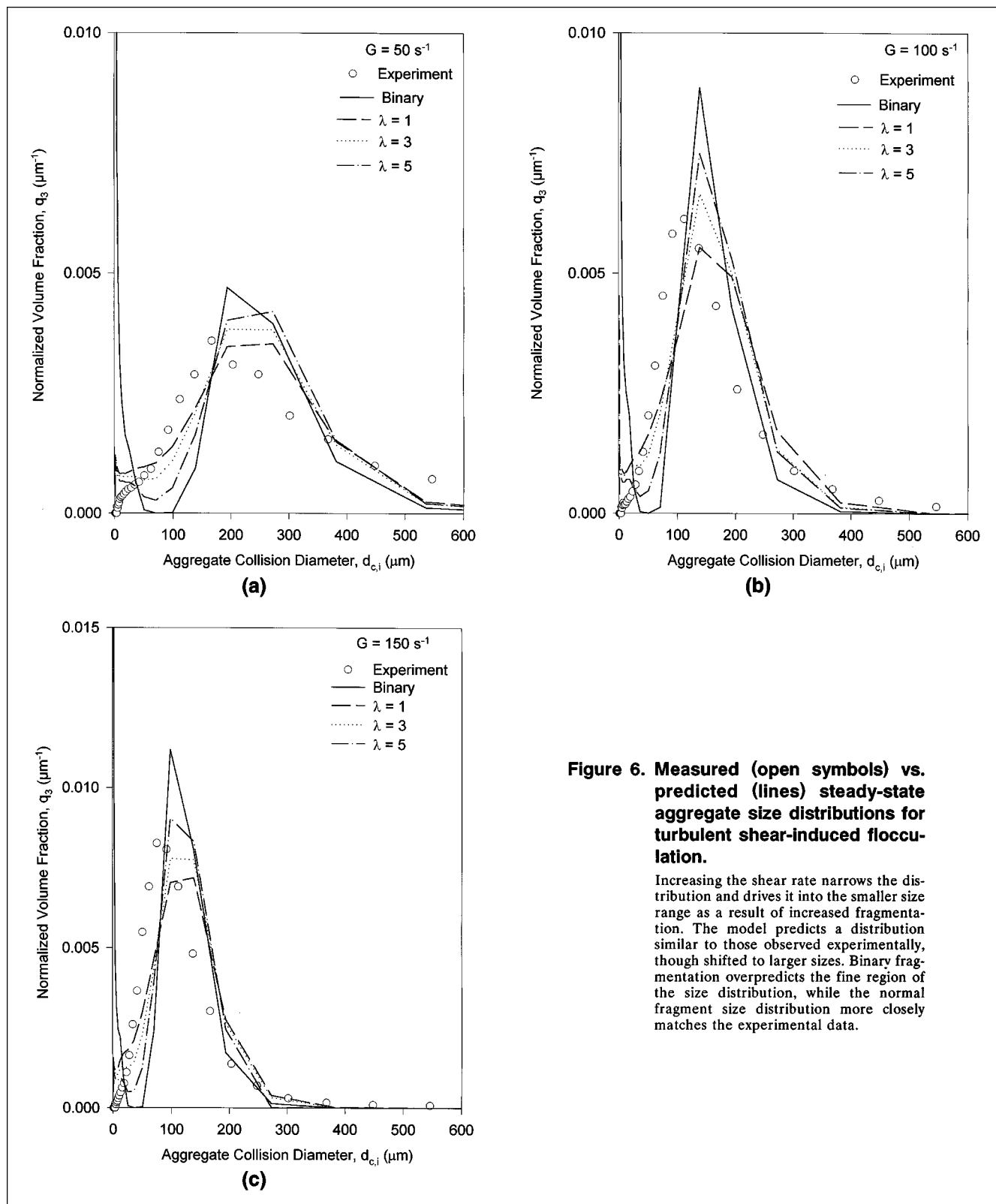


Figure 6. Measured (open symbols) vs. predicted (lines) steady-state aggregate size distributions for turbulent shear-induced flocculation.

Increasing the shear rate narrows the distribution and drives it into the smaller size range as a result of increased fragmentation. The model predicts a distribution similar to those observed experimentally, though shifted to larger sizes. Binary fragmentation overpredicts the fine region of the size distribution, while the normal fragment size distribution more closely matches the experimental data.

Figure 6

fragmentation rates, in agreement with theory (Spicer and Pratsinis, 1996a). The theoretical volume distributions for each shear rate are plotted as lines for binary breakage as well as several forms of the normal fragment size distribu-

tion. In order to compare the experimental data with the theoretical size distributions, the volume fractions in each section must be divided with the section width, since the sectional spacing differs in both cases (Hinds, 1982).

For binary fragmentation, the large-particle modes of the modeled size distributions at all three shear rates have similar shapes to those found in the experiment, though their peaks are slightly shifted to larger aggregate sizes. In the model, there are still particles in the low size range ($d_{c,mm} \leq 10 \mu\text{m}$), whereas experimentally no such particles are detected (though it should be noted that the Malvern may not fully detect such fine particle modes if they are present). Although there is a size range at all three shear rates (between 50- and 100- μm aggregate diameter) in which the model predicts no particles, a considerable amount of particles are found there experimentally for all three shear rates. Binary fragmentation, although simple to implement theoretically, clearly produces a steady-state aggregate size distribution significantly different from that observed experimentally. Observations of aggregate disintegration under shear also indicate that the binary fragmentation assumption is an oversimplification. It should, however, be emphasized that excellent agreement is observed between theoretical and experimental average aggregate-size evolution with a minimum of fitting. As a result, binary fragmentation may provide adequate modeling accuracy, depending on the level of predictive detail desired. More detailed matching of aggregate-size distributions requires alternative model formulation.

Spicer and Pratsinis (1996a) showed that a broadened fragment-size distribution function broadened the shape of the steady-state particle-size distribution during simultaneous coagulation-fragmentation. Assuming a normally distributed breakage function instead of binary breakage, the steady-state size distribution is broadened toward smaller particles (Spicer and Pratsinis, 1996a). The fragment-size distribution standard deviation is influenced by choosing appropriate values for λ in Eq. 12. The larger the λ , the narrower the fragment-size distribution. In contrast, the smaller the λ , the broader the fragment-size distribution. As a result, decreasing λ broadens the steady-state size distribution and increases the amount of smaller particles formed by fragmentation.

In Figure 6, binary aggregate fragmentation produces a bimodal size distribution that does not match the unimodal one observed experimentally. Fragmentation is clearly overpredicted. The flexibility of the normal fragment-size distribution allows the steady-state size distribution to be narrowed to optimize comparison with experimental data. In Figure 6, for three values of λ (1, 3, and 5) the steady-state size distributions are narrower than those produced for binary fragmentation. As a result, the agreement with experimental data is improved significantly. However, the model still overpredicts the percentage of the distribution composed of smaller particles. The discrepancy may result from a respective over- or underprediction of coagulation or fragmentation rates, or both. The coagulation rate is calculated using the maximum aggregate diameter (Eq. 3) and may overestimate the actual aggregate collision profile, depending on the aggregate structure and orientation (Spicer, 1998). In addition, this model does not account for the heterogeneity of the stirred tank. Fragmentation in a stirred tank occurs most in the impeller zone, a relatively small area with a high shear rate (Kusters, 1991). On the other hand, coagulation occurs most in the bulk (nonimpeller) zone, an area with lower shear rates than average. The volume-averaged shear rate used here may thus overestimate the actual coagulation rate and underestimate

the fragmentation rate depending on the aggregate residence time distribution in each zone. Finally, the average aggregate fractal dimension has been shown to change during flocculation by restructuring (Oles, 1992), and this may also partially explain the observed discrepancies as the model assumes a constant D_f . Regarding a comparison with the experimental data, a value of λ equal to 3 seems to give the best agreement. With λ , a second fitting parameter becomes necessary.

Evolution of size distribution

It is also interesting to compare the model predictions with the experimental size distribution evolution. Figure 7 compares theoretical and experimental size distributions at four different flocculation times ($t = 6, 8, 14,$ and 27 min) for $G = 50 \text{ s}^{-1}$. For illustration purposes the normally distributed breakage function was applied here with $\lambda = 3$ (Spicer and Pratsinis, 1996a) for the reasons just given. In Figure 7, the agreement between model and experiments is best as short times as a result of the fixed initial conditions. At short coagulation times (Figure 7a), the modeled distributions are of a comparable width to the experimental ones, although the model predicts a more unimodal distribution. At longer times, however (Figures 7b-7c), the model develops a bimodal character as the experimental data begin to exhibit unimodal behavior. Observation of Figure 7 indicates better model agreement with the coarse region of the size distribution data at longer times. In light of the fact that the sole fitting of the model to the data was carried out by comparison with the steady-state mass averaged size (Figure 4), it is not surprising that the results are biased toward the coarse portion of the particle-size distribution. This bias offers some degree of choice in the part of the distribution of most interest to follow, depending on the desire for control of fine or coarse particles. The two other shear rates ($G = 100 \text{ s}^{-1}$ and 150 s^{-1}) exhibit similar size distribution comparisons (i.e., overprediction of fine particle population). It should also be noted that upon recomparison of the experimental data for the evolution of $d_{c,mm}$, little change is observed between model runs, assuming binary and normal fragment-size distribution schemes.

Comparison between model and literature data for laminar shear

It is also of interest to compare this model with additional existing measurements to determine its applicability in different flow regimes. Oles (1992) carried out flocculation experiments in a laminar shear Couette apparatus ($G = 25\text{--}150 \text{ s}^{-1}$) using NaCl to destabilize a monodisperse, polystyrene latex suspension with $d_0 = 2.17 \mu\text{m}$ and an initial solids volume fraction of $\phi = 5 \times 10^{-5}$. The particle size distributions were then measured by light scattering (Malvern Mastersizer). Spicer and Pratsinis (1996a) modeled these data using a simplified form of the present model that lumped together aggregate structure and viscous effects into a collision efficiency of $\alpha = 1$. They acknowledged that this value was artificial, but worked well to account for the competing effects of aggregate structure and fluid viscosity on flocculation kinetics. Oles (1992) reports an average value for the $D_f = 2.3$. This value was used here for all shear rates to model the

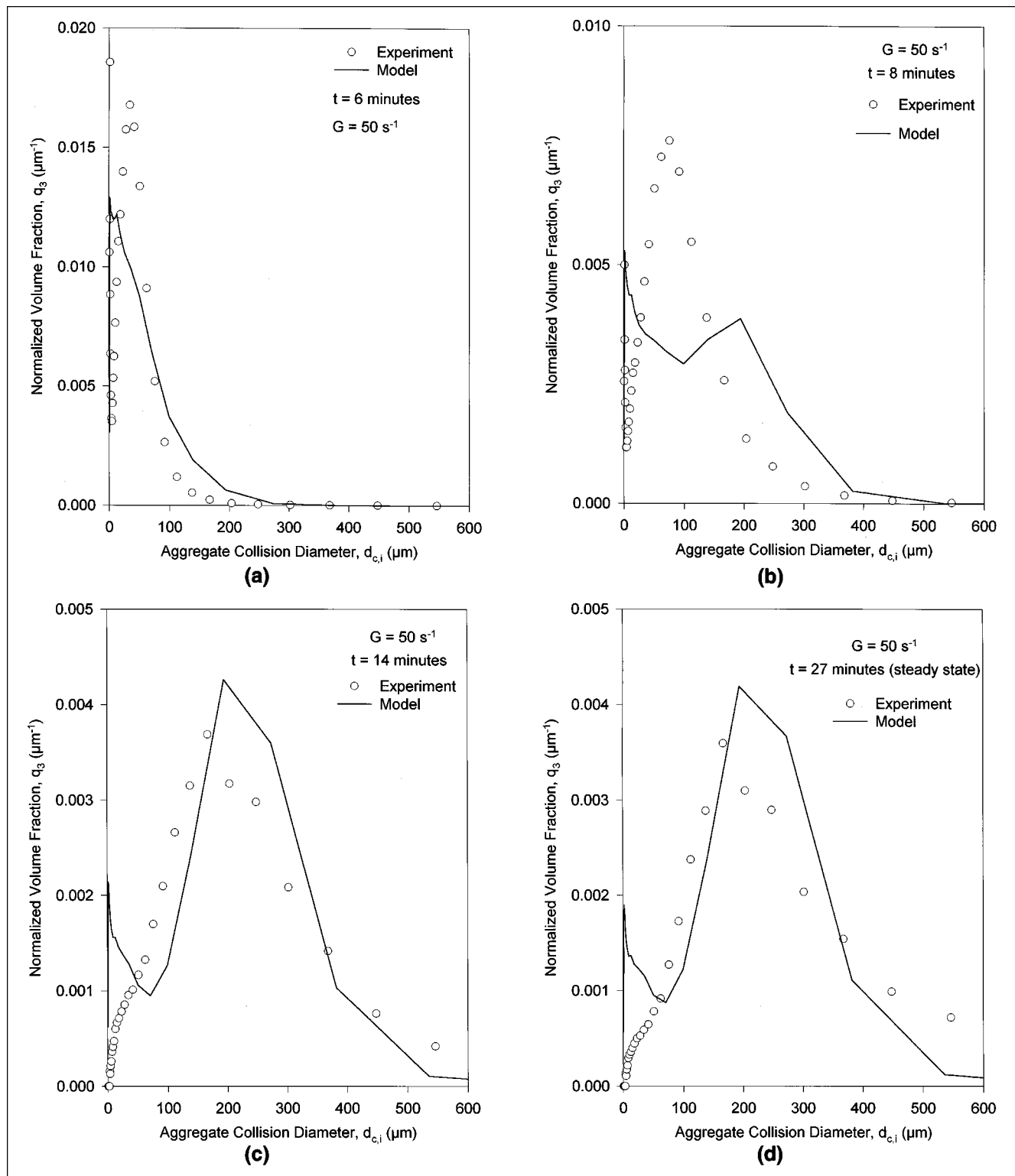


Figure 7. Evolution of measured (open circles) aggregate size distributions vs. prediction by the model (solid line). It indicates a net overprediction of aggregation rates. As a result, broader distributions than those measured are predicted.

data, as shown in Figure 8. The steady state for each shear rate was reached by adjusting B , as described previously. As such, the agreement between model and experiment is good for all shear rates. The size evolution of the aggregates shows

the same behavior for laminar shear as for turbulent shear. The initial exponential increase is slowed down by fragmentation until a steady state is reached. The fitting parameter can be correlated by a power law (Spicer and Pratsinis, 1996a).

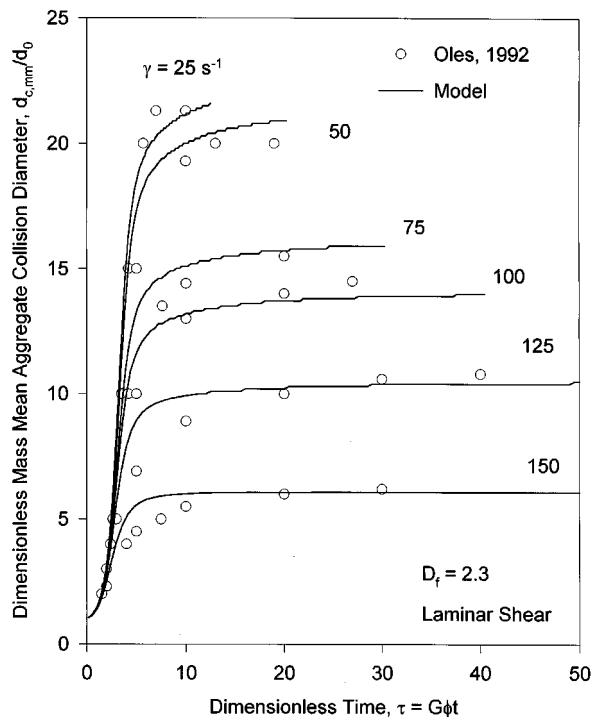


Figure 8. Time evolution of the mass mean aggregate diameter for experimental (open symbols) and theoretical (solid lines) values of laminar shear-induced aggregation.

The theoretical lines were produced by numerical solution of Eq. 1 using Eq. 5 modified for laminar shear flow. The same trends are observed for laminar shear as for turbulent shear, concluding in the attainment of a steady-state aggregate size. The model (using only one fitting parameter, B) is also in excellent agreement with the laminar results.

The power law found for this data set is given by

$$B = A' G^y. \quad (17)$$

The value of A' was found to equal 7×10^{-4} and the value of $y = 1.6$. The value of y is identical to the 1.6 found by Spicer and Pratsinis (1996a); however, the value of A' is about seven times smaller than theirs ($A' = 0.0047$). The reason for this is the different fragmentation law used herein.

Conclusions

A sectional population balance model was developed that accounts for aggregate structure and hydrodynamic effects on flocculation. The model was found to describe quite well the evolution of the mass mean aggregate diameter during turbulent shear-induced flocculation in a stirred tank. In addition, its applicability to modeling flocculation in laminar shear was also demonstrated, again using experimentally determined D_f values.

Reasonable agreement was observed between the experimental and predicted evolution of aggregate-size distributions during turbulent shear flocculation for all shear rates. Agreement between theory and experiment was improved by applying a normal fragment-size distribution. Thus, the inclu-

sion of viscous retardation and aggregate structure gives a more detailed picture of flocculation kinetics than earlier models that only considered spherical structures and inviscid fluid. However, the heterogeneity of the flow field has not been considered in this model. The agreement between this model and experimental data imply that the approximation of the turbulent shear field with a volume-averaged shear rate and constant mass fractal dimension is justified for time-averaged quantities, while particle-size distributions are predicted with less accuracy.

Acknowledgments

The support of this research by The Procter & Gamble Company and the University of Cincinnati, Cincinnati, Ohio, is gratefully acknowledged. The authors are also grateful for access to the particle characterization expertise and equipment of Professor Judy Raper, Dr. Rose Amal, and Dr. Graeme Bushell (University of New South Wales, Sydney, Australia).

Notation

- A' = fragmentation-rate coefficient relating fragmentation rate to shear rate
- $d_{c,i}$ = collision diameter of an aggregate, μm
- i = number of primary particles in an aggregate
- max_1 = index of the largest section undergoing aggregation
- max_2 = index of the largest fragmenting particle
- t = time, s
- y = experimentally determined coefficient in Eq. 17

Literature Cited

- Adler, P. M., "Streamlines in and Around Porous Particles," *J. Colloid Interf. Sci.*, **81**, 531 (1981a).
- Adler, P. M., "Heterocoagulation in Shear Flow," *J. Colloid Interf. Sci.*, **83**, 106 (1981b).
- Adler, P. M., and P. M. Mills, "Motion and Rupture of a Porous Sphere in a Linear Flow Field," *J. Rheol.*, **23**, 25 (1979).
- Clark, M. M., and J. R. V. Flora, "Floc Restructuring in Varied Turbulent Mixing," *J. Colloid Interf. Sci.*, **147**, 407 (1991).
- Delichatsios, M. A., and R. F. Probstein, "The Effect of Coalescence on the Average Drop Size in Liquid-Liquid Dispersions," *Ind. Eng. Chem. Fundam.*, **15**, 134 (1976).
- Francois, R. J., "Strength of Aluminum Hydroxide Floccs," *Water Res.*, **21**, 1025 (1987).
- Hinds, W. C., *Aerosol Technology*, Wiley-Interscience, New York (1982).
- Horwath, S. W., D. L. Feke, and I. Manas-Zloczower, "The Influence of Structural Heterogeneities on the Cohesivity and Breakup of Agglomerates in Simple Shear Flow," *Powder Technol.*, **72**, 113 (1992).
- Hounslow, M. J., R. L. Ryall, and V. R. Marshall, "A Discretized Population Balance for Nucleation, Growth, and Aggregation," *AIChE J.*, **34**, 1821 (1988).
- Jiang, Q., and B. E. Logan, "Fractal Dimensions of Aggregates Determined from Steady State Size Distributions," *Environ. Sci. and Technol.*, **25**, 2031 (1991).
- Klimpel, R. C., and R. Hogg, "Effects of Flocculation Conditions on Agglomerate Structure," *J. Colloid Interf. Sci.*, **113**, 121 (1986).
- Kusters, K. A., "The Influence of Turbulence on Aggregation of Small Particles in Agitated Vessels," Ph.D. Diss., Eindhoven Univ. of Technology, Eindhoven, The Netherlands (1991).
- Kusters, K. A., J. G. Wijers, and D. Thoenes, "Aggregation Kinetics of Small Particles in Agitated Vessels," *Chem. Eng. Sci.*, **52**, 107 (1997).
- Mandelbrot, B. B., *The Fractal Geometry of Nature*, Freeman, New York (1987).
- Meakin, P., "Fractal Aggregates," *Adv. Colloid Interf. Sci.*, **28**, 249 (1988).

- Ng, K. W. K., R. Amal, J. A. Raper, and T. D. Waite, "The Effects of Alum Concentration and pH on the Aggregation Kinetics of Colloidal Haematite," *Proc. Int. Symp. on Agglomeration*, Nagoya, Japan, p. 785 (1993).
- Oles, V., "Shear-Induced Aggregation and Breakup of Polystyrene Latex Particles," *J. Colloid Interf. Sci.*, **154**, 351 (1992).
- Potantin, A. A., "On the Mechanism of Aggregation in the Shear Flow of Suspensions," *J. Colloid Interf. Sci.*, **145**, 140 (1991).
- Saffman, P., and J. Turner, "On the Collision of Drops in Turbulent Clouds," *J. Fluid Mech.*, **1**, 16 (1956).
- Schmidt-Ott, A., U. Baltensperger, H. W. Gaggeler, and D. T. Jost, "Scaling Behavior of Physical Parameters Describing Agglomerates," *J. Aerosol Sci.*, **21**, 711 (1990).
- Smoluchowski, M., "Versuch Einer Mathematischen Theorie de Koagulations-Kinetik Kolloider Losungen," *Z. Phys. Chem.*, **92**, 129 (1917).
- Sonntag, R. C., and W. B. Russel, "Structure and Breakup of Floccs Subjected to Fluid Stresses I. Shear Experiments," *J. Colloid Interf. Sci.*, **113**, 399 (1986).
- Sonntag, R. C., and W. B. Russel, "Structure and Breakup of Floccs Subjected to Fluid Stresses II. Theory," *J. Colloid Interf. Sci.*, **115**, 378 (1987).
- Spicer, P. T., and S. E. Pratsinis, "Coagulation-Fragmentation: Universal Steady State Particle Size Distributions," *AIChE J.*, **42**, 1612 (1996a).
- Spicer, P. T., and S. E. Pratsinis, "Shear-Induced Flocculation: The Evolution of Floc Structure and the Shape of the Size Distribution at Steady State," *Water Res.*, **30**, 1049 (1996b).
- Spicer, P. T., S. E. Pratsinis, J. A. Raper, R. Amal, G. Bushell, and G. Meesters, "Effect of Shear Schedule on Particle Size, Density, and Structure during Flocculation in Stirred Tanks," *Powder Technol.*, **97**, 26 (1998).
- Spicer, P. T., "Shear-Induced Aggregation-Fragmentation: Mixing and Aggregate Morphology Effects," PhD Diss., Univ. of Cincinnati, Cincinnati, OH (1998).
- Tambo, N., and Y. Watanabe, "Physical Aspect of Flocculation Process: I. Fundamental Treatise," *Water Res.*, **13**, 429 (1979a).
- Tambo, N., and Y. Watanabe, "Physical Characteristic of Floccs: I. The Floc Density Function and Aluminum Floc," *Water Res.*, **13**, 409 (1979b).
- Thomas, D. G., "Turbulent Disruption of Floccs in Small Particle Size Suspensions," *AIChE J.*, **10**, 517 (1964).
- Tomi, D. T., and D. F. Bagster, "The Behaviour of Aggregates in Stirred Vessels, Part 1—Theoretical Considerations on the Effects of Agitation," *Trans. Inst. Chem. Eng.*, **56**, 1 (1978).
- Torres, F. E., W. B. Russel, and W. R. Schowalter, "Simulations of Coagulation in Viscous Flows," *J. Colloid Interf. Sci.*, **145**, 51 (1991).
- Vigil, R. D., and R. M. Ziff, "On the Stability of Coagulation-Fragmentation Population Balances," *J. Colloid Interf. Sci.*, **133**, 257 (1989).
- Wiesner, M. R., "Kinetics of Aggregate Formation in Rapid Mix," *Water Res.*, **26**, 379 (1992).

Manuscript received Nov. 17, 1998, and revision received Mar. 25, 1999.